

Fabrication of a 60-nm-Diameter Perfectly Round Metal-Dot Array over a Large Area on a Plastic Substrate Using Nanoimprint Lithography and Self-Perfection by Liquefaction

Chao Wang, Qiangfei Xia, Wen-Di Li, Zengli Fu, Keith J. Morton, and Stephen Y. Chou*

Typically, nanopatterning on plastic substrates has poor fidelity, poor adhesion, and low yield. Here the proposal of and the first experiment using a new fabrication method that overcomes the above obstacles and has achieved arrays of 60-nm-diameter, perfectly round metal dots over a large area on a polyethylene terephthalate (PET) substrate with high fidelity and high yield is reported. This new method is based on the use of a thin hydrogen silsesquioxane (HSQ) layer on top of PET, nanoimprint lithography, and self-perfection by liquefaction (SPEL). The HSQ layer offers excellent thermal protection to the PET substrate during SPEL, as well as good surface adhesion and etching resistance. Nanoimprinting plus a lift off created a large-area array of Cr squares (100 nm × 130 nm) on HSQ and SPEL changed each Cr square into a perfectly round Cr dot with a diameter of 60 nm, reducing the Cr footprint area by 78%. Compared to bare PET, the use of HSQ also reduced the variation in the diameter of the Cr dots from 11.3 nm (standard deviation) to 1.7 nm, an improvement of over 660%. This new technology can be scaled to much larger areas (including roll-to-roll web processing) and thus potentially has applications in various fields.

Keywords:

- liquefaction
- nanoimprint lithography
- nanopatterning
- plastic substrates

1. Introduction

Plastic substrates are desirable for many future portable, flexible, and transparent electronics,^[1–3] such as light-emitting diodes (LEDs),^[1] displays,^[3] transistors,^[4] and solar cells.^[5] However, compared with hard solid substrates, plastic substrates have a number of problems during direct nanopatterning, such as poor etching resistance,^[6] weak adhesion,^[7] easy deformation (i.e., small elastic modulus^[8]), and a low melting temperature,^[9] all of which lead to poor patterning quality.^[10]

Herein, we propose and demonstrate a new fabrication method that has achieved 60-nm-diameter perfectly round metal-dot arrays (235-nm pitch) over a large area on a polyethylene terephthalate (PET) substrate with high fidelity and high yield. The method has three key novel aspects. Firstly, a thin (≈ 450 nm) high-melting-temperature (at least >1100 °C^[11]) material, hydrogen silsesquioxane (HSQ), was used as the surface layer on top of the plastic substrate, which offers good adhesion to both the plastic substrate and the metal dots, a significantly enhanced etching resistance to the substrate, a stable and nonmelting surface to the Cr dots during self-perfection by liquefaction (SPEL), and excellent heating protection (during SPEL) to the underlying PET substrate. Secondly, nanoimprint lithography (NIL)^[12,13] and lift off were used to pattern the initial metal-nanostructure array on plastic over a large area (can be scaled up to meters or large sizes). Thirdly, SPEL^[14] was used to reshape the initial

[*] C. Wang, Dr. Q. Xia, W.-D. Li, Z. Fu, K. J. Morton, Prof. S. Y. Chou
Nanostructure Laboratory Department of Electrical Engineering
Princeton University, NJ 8544(USA)
E-mail: chou@princeton.edu

noncircularly patterned metal array into the dot array with a reduced lateral dimension (uniform 60-nm diameter) and a perfectly round and smooth shape, which we believe cannot be achieved by other technologies.

2. Results and Discussion

2.1. Procedure of Cr Nanodot Patterning

Our approach consists of the following five detailed steps (Figure 1): (a) cleaning of a $\approx 100\text{-}\mu\text{m}$ -thick PET film (Melinex 454, Dupont Teijin Films) with methanol/isopropanol, followed by oxygen plasma at 50 W and 10 mtorr for 2 min (Plasma Therm SLR 720) to facilitate the subsequent HSQ coating on PET; (b) spin coating HSQ (Gelest, Inc.) on the PET, followed by baking at $110\text{ }^\circ\text{C}$ overnight in ambient air to drive off the solvent in the HSQ film (to achieve a final thickness of $\approx 450\text{ nm}$); (c) oxygen-plasma treatment of the HSQ film at 50 W and 10 mtorr for 2 min, spin coating the double-layer UV-imprint resist (Nanonex Corp.), and then nanoimprinting for 3 min at 200 psi and room temperature with 15-s UV illumination using a fused silica pillar mold (235-nm pitch, pillar size = $110\text{ nm} \times 140\text{ nm}$) of about $30\text{ mm} \times 30\text{ mm}$ size; (d) reactive ion etching (RIE) of residual imprint resist and then e-beam evaporation (BJD 1800, Temescal) and lift off (spraying methanol/deionized water with a 1:1 ratio) to pattern Cr dots; and (e) open-space SPEL^[14] using a 20-ns (full width at half maximum) single pulse of a 308-nm XeCl excimer laser (Compex 102, Lambda Physik) to melt and reshape the Cr dots.

The double-layer resist used in step (c) consists of two layers: a low-viscosity UV-curable resist ($\approx 110\text{ nm}$ thick) on top

and a water-soluble polymer ($\approx 250\text{-nm}$ thick) on the bottom. The top resist residual layer was removed by O_2/CHF_3 plasma (1.5/10 sccm, 15 mtorr, 100 W, etching rate $\approx 15\text{ nm min}^{-1}$) in a Plasma Therm SLR 720 and the bottom resist residual layer was then removed by O_2 plasma (10 sccm, 10 mtorr, 50 W, $\approx 40\text{ nm min}^{-1}$). The use of a double-layer resist offers a deep resist profile and easy dissolution of the resist. Both are beneficial for a successful lift off without using harsh resist removals (e.g., ultrasonic agitation or an oxidizer-based resist remover) to avoid pattern distortion, substrate damage, and poor adhesion.

2.2. Cr Dots Patterned by NIL and SPEL with a HSQ Underlayer

Comparing scanning electron microscopy (SEM) images of the NIL mold (Figure 2a) and imprinted resist (Figure 2b), we can see that the large-area uniformity of the patterns was preserved during imprinting. Figure 2c and d shows that the

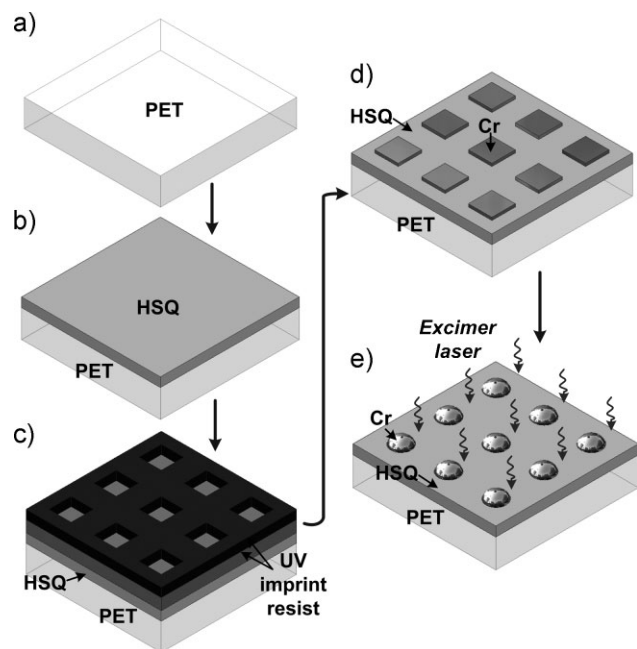


Figure 1. Schematics of the fabrication of uniformly patterned metal-dot arrays on a PET substrate using a HSQ coating, NIL, and SPEL: a) a PET film and cleaning; b) spin coating a thin layer of HSQ onto PET; c) UV NIL with a pillar mold; d) RIE, evaporation of Cr metal, and lift off; e) open SPEL to perfect the shape of the Cr dots.

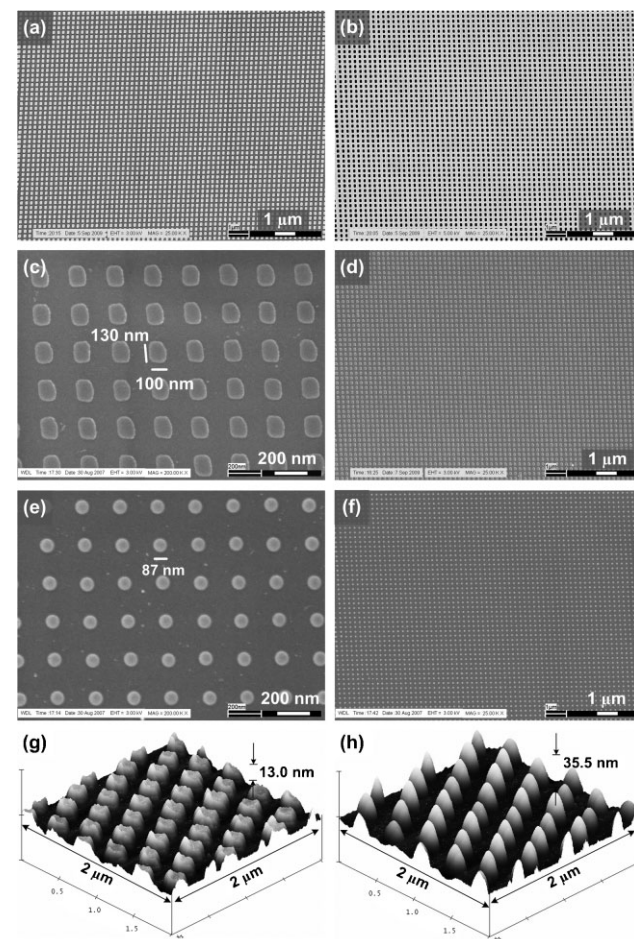


Figure 2. Cr dots array uniformly patterned on HSQ-coated PET substrate using NIL and SPEL. SEM images of: a) original 235-nm period NIL mold fabricated in fused silica and b) as-imprinted patterns in double-layer resist. c, d) SEM images of NIL-patterned Cr squares ($100\text{ nm} \times 130\text{ nm}$). e, f) SEM images of 87-nm-diameter round Cr dots reshaped by SPEL (single pulse, 168 mJ cm^{-2}) with good uniformity over a large area ($5.5\text{ mm} \times 5.5\text{ mm}$). AFM images of the surface topography of Cr dots with and without SPEL: g) 13-nm-high as-patterned squares (SEM images in (c) and (d)) and h) 35.5-nm-high round particles after SPEL (SEM images in (e) and (f)).

resist patterns were transferred to Cr squares ($100 \times 130\text{-nm}^2$ area and 235-nm period) with a good fidelity and over a large area (Figure 2d). Figure 2e shows that SPEL successfully reshaped each Cr square into a single dot, which not only had a nearly perfectly round hemisphere but also a diameter ($87 \pm 2\text{ nm}$) significantly smaller than the original one (dot area on the substrate reduced by 55%). On the other hand, the location of the center of the Cr dots did not change after processing, strongly indicating that the adhesion between Cr and HSQ is excellent. This is because HSQ has a surface energy similar to SiO_2 (typically $\approx 1\text{--}2\text{ J m}^{-2}$ ^[15]) after oxygen plasma treatment^[16] due to the modification of the surface with hydroxyl groups^[17,18] and thus wets molten Cr well. Figure 2f shows that our patterning technology can achieve good uniformity over a large area, which was about $5.5 \times 5.5\text{ mm}^2$ by stitching adjacent exposed regions^[19] and could be extended to a much large area by a scanning laser beam.

Atomic force microscopy (AFM) of the surface of the Cr dots before and after SPEL on HSQ/PET (Figure 2g and h) shows that the height of the metal particles after SPEL was increased from $\approx 13.0\text{ nm}$ to $\approx 35.5\text{ nm}$, while the lateral diameter was decreased (SEM images of Figure 2c–f), but the total volume of the Cr dots was kept constant.

2.3. Comparison with Cr Nanodots Patterned Without a HSQ Underlayer

In contrast, when a HSQ layer was not used, the fabrication of Cr dots on bare PET had very poor yield and poor control of the sizes, shapes, and locations of the dots. For example, oxygen plasma could overetch into the PET substrate, creating deep craters (Figure 3a). PET has a poor etching resistance^[6] and an etching rate (20 nm min^{-1}) comparable to the NIL bottom resist ($\approx 40\text{ nm min}^{-1}$) under the same etching conditions (RIE at 50 W in Plasma-Therm SLR 720). Therefore, a slight $\approx 1\text{--}2\text{-min}$ overetch of NIL resist, which is necessary for overcoming the nonuniformities in resist thickness and RIE etching rate while ensuring total removal of the resist, would inevitably lead to $\approx 20\text{--}40\text{-nm}$ deep pits in PET. This resulted in the Cr dots patterned in the PET craters (Figure 3a). On the other hand, if there was no overetching, the nonuniformities of the resist thickness and RIE would leave a resist residue in some of the etched holes, which would cause the Cr dots deposited inside these holes to be missing during the lift off (Figure 3b).

Moreover, the laser energy in SPEL (151 and 168 mJ cm^{-2} in Figure 3c and d, respectively) melted not only the Cr dots but also the PET film. Furthermore, due to incompatibility of the surface energies (1.6 J m^{-2} for Cr^[20] and 60 mJ m^{-2} for PET^[21]), PET does not wet molten Cr. This made the molten Cr droplets move around on the PET surface to random locations, significantly destroying the periodic array. Finally, the movement of the Cr droplets could cause an agglomeration of several dots to form large-diameter, noncircular, and nonuniform dots (Figure 3d).

From the results above, it becomes clear that the superior results with a HSQ layer over a bare PET substrate are due to HSQ's a) high melting temperature, which not only guarantees that HSQ doesn't melt during the processes but also prevents

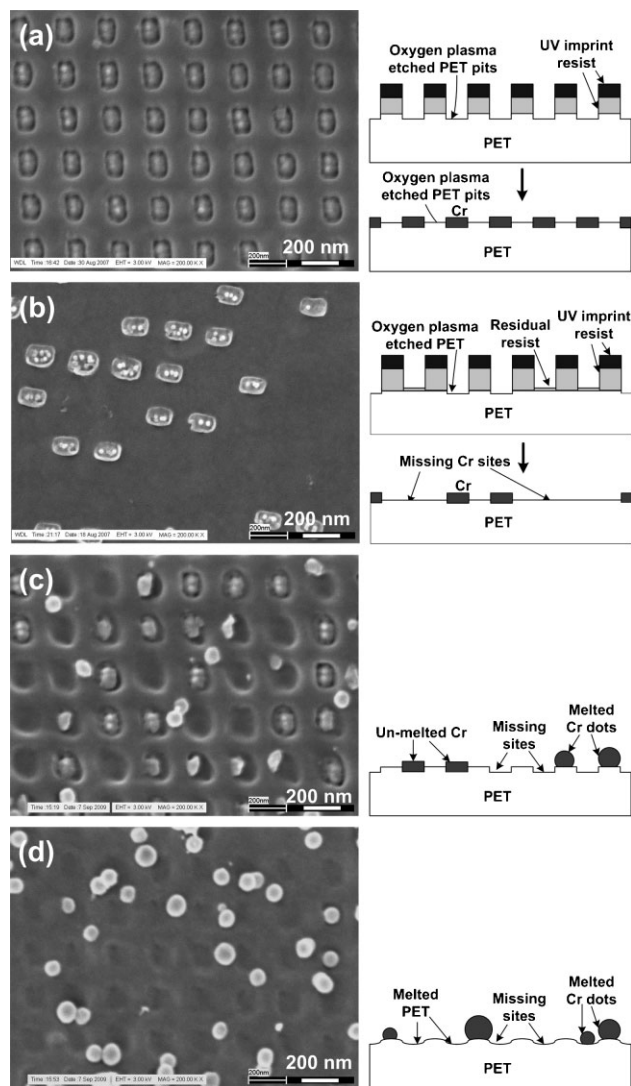


Figure 3. SEM images (left column) and schemes (right column) of poorly patterned Cr dots on bare PET using NIL and SPEL. a) Cr dots obtained in recessed PET pits after overetching residual resist with oxygen plasma, Cr evaporation, and lift off. b) Cr dots with missing sites after insufficient plasma etching of residual resist, followed by the same evaporation and lift off. Melted Cr dots (both originally patterned as in (a) with random locations and different diameters after SPEL: c) partial melting with SPEL at 151 mJ cm^{-2} ; d) complete melting at 168 mJ cm^{-2} .

the PET below from melting, b) high O_2 -etching resistance, c) wetting to molten Cr, and d) excellent surface adhesion to Cr.

To quantify the nanopatterning fidelity with and without a thin HSQ layer, the diameter distributions of the Cr dots were calculated, as shown in Figure 4. It can be seen that Cr dots on HSQ-coated PET had a diameter deviation of 1.7 nm (calculated from Figure 2e), which is over 660% less than 11.3 nm , the diameter deviation of the Cr on bare PET (i.e., without a HSQ layer) (calculated from Figure 3d). As can be clearly seen from the inset SEM images, the Cr dots melted on HSQ/PET were hemisphere-like, while those on bare PET were spherical. The difference originates from the different surface energies of the HSQ (close to $\approx 1\text{--}2\text{ J m}^{-2}$ ^[15]) and bare PET (60 mJ m^{-2} ^[21]). As a result, the molten Cr had a small

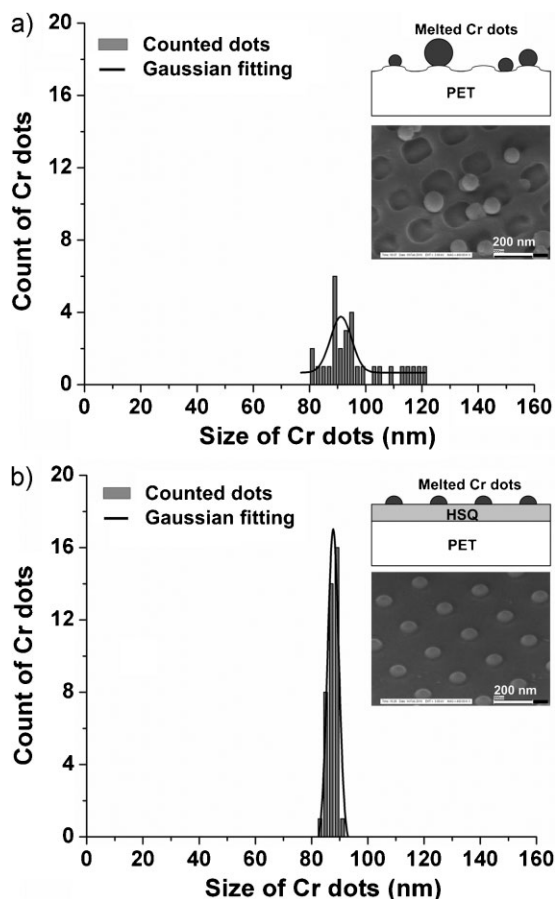


Figure 4. Diameter distributions of Cr dots on bare PET and HSQ-coated PET after NIL and SPEL: a) 11.3 nm (standard deviation) for Cr dots on bare PET and b) 1.7 nm for the Cr dots on HSQ/PET, showing over 660% improvement. The cross-sectional schematics and side-view SEM images are shown inset.

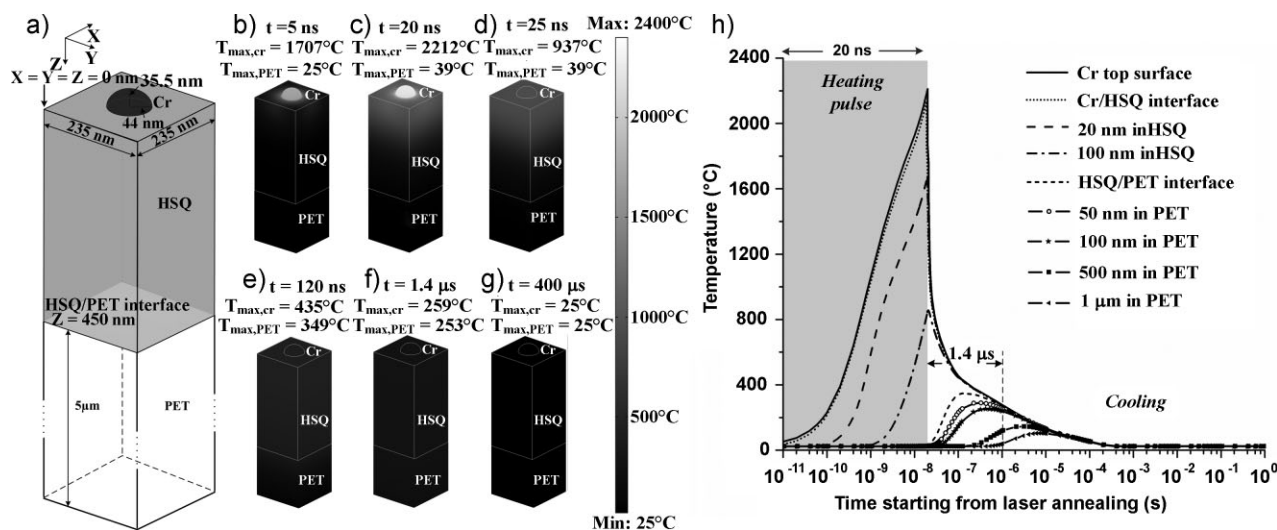


Figure 6. COMSOL simulation to analyze the spatial distribution and transient variation of temperatures within a Cr/HSQ/PET structure during annealing (20-ns duration, 168 mJ cm^{-2}) and subsequent cooling. a) The model used in simulation, with the geometrical dimensions being the same as the experimental parameters except for the thickness of PET (assumed here to be $5 \mu\text{m}$). Spatial temperature distributions at different time after initializing annealing, with the peak values of Cr ($T_{\text{max,Cr}}$) and PET ($T_{\text{max,PET}}$) given for reference: b) 5 ns, c) 20 ns, d) 25 ns, e) 120 ns, f) 1.4 μs , and g) 400 μs . h) Transient temperature variation at different depths along the axis of symmetry ($x=y=117.5 \text{ nm}$), clearly showing the role of HSQ in thermally insulating PET from heat damage. The convective heat transfer coefficient is assumed to be $50 \text{ W m}^{-2} \text{ K}^{-1}$.

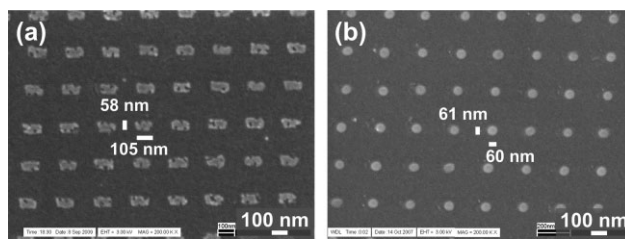


Figure 5. SEM images of Cr dots on HSQ/PET with smaller diameters before and after SPEL, showing the capabilities of SPEL in reducing line-edge roughness and shrinking the diameters of metal dots. a) ≈ 10 -nm-thick Cr dots ($105 \pm 5 \text{ nm} \times 58 \pm 4 \text{ nm}$) patterned on HSQ/PET after four-time shadow evaporation of Cr (65° to the substrate surface, $\approx 15 \text{ nm}$ each direction), RIE, Cr evaporation normal to PET, and lift off. Clearly, the Cr pads have very rough edges and asymmetric shapes. b) Nearly perfectly round Cr dots ($61 \pm 3 \text{ nm} \times 60 \pm 3 \text{ nm}$) obtained on HSQ/PET after SPEL using a single laser pulse (277 mJ cm^{-2}). This corresponds to an area reduction from the original patterns of 80%.

contact angle and was wet on HSQ surfaces, while Cr dewetted on PET, hence being spherical in shape.

Clearly, the diameter of the Cr dots can be reduced by making the initial Cr squares smaller and/or thinner.^[19] As shown in Figure 5, 60-nm-diameter nearly perfectly round Cr dots were fabricated on HSQ/PET.

3. Numerical Simulation of the Transient Temperature Distribution of the Cr/HSQ/PET Structure

To understand the temperatures of each material during SPEL, we performed numerical simulations using a commercial software package (COMSOL). The structure symmetry reduces the calculation to one unit cell with a size of $235 \text{ nm} \times 235 \text{ nm}$ with a Cr partial sphere (height = 35.5 nm, radius = 44 nm) at the center of the cell (Figure 6a). The

simulation used the same geometry of HSQ and Cr as in experiment but we assumed a 5- μm thickness for PET, which should not affect the simulation accuracy since PET is a poor thermal conductor^[22] and hence would not propagate heat deeply. The parameters for each material at different temperatures were taken from the literature,^[9,22,23] except for the temperature-dependent properties of PET (which were not available) and the properties of HSQ (not available, assumed to be the same as SiO_2).

From simulation of the spatial temperature distribution (Figure 6b–g) and transient temperature variation (Figure 6h) inside the Cr/HSQ/PET structure, it is shown that the highest temperatures were 2212 °C (above 1907 °C, the melting point of bulk Cr) at the Cr top surface and 2137 °C at the Cr/HSQ interface but that they lasted for only ≈ 5 ns and cooled off quickly. The highest temperature at the HSQ/PET interface was only 350 °C for several hundred nanoseconds. The time span of PET at the temperatures above 260 °C was less than 1.4 μs (Figure 6f). This shows that the HSQ acted well as a thermal-barrier layer to suppress the maximum temperature and heating time of the PET substrate. For the structure with Cr/PET only (i.e., without HSQ), the Cr dot in the molten state not only liquefied the PET but could also vaporize it, causing the Cr dots to move randomly, as observed experimentally.

4. Thermal Stability of the Cr/HSQ/PET Structure During the SPEL Process

The stability of the multilayer Cr/HSQ/PET film during the SPEL process is a critical issue for many applications as rapid heating of Cr to >1900 °C could cause thermally induced buckling/delamination and/or degrade the film quality. However, we have not observed any such degradation issues in our experiments with a HSQ underlayer (Figure 4a). The possible reasons for this are that (a) oxygen-plasma treatment of HSQ^[16] and PET^[6] enhances the film surface energies and adhesion and/or (b) our simulation shows that the heating is limited in temperature, duration, and film depth (e.g., only the top 0.1% for PET).

5. Conclusions

In summary, we have proposed and demonstrated a new approach to pattern 2D metal (Cr) arrays of uniform 60-nm diameter on a PET substrate using NIL and SPEL. We have demonstrated that a layer of HSQ is essential to achieve reliable patterning on PET by experimentally comparing NIL and SPEL results with and without HSQ coating. With the HSQ layer, SPEL was capable of greatly reducing the pattern roughness as well as reducing the pattern size ($\approx 80\%$ using shadow evaporation). Besides experimental investigations, numerical simulation was used to confirm that the HSQ layer could effectively lower the thermal budget of the plastic substrate by greatly reducing the peak temperatures and shortening the duration of heating. Our approach of using a spin-on glass^[24] (HSQ in our case) to integrate NIL and SPEL into feature patterning on a plastic substrate is simple, reliable, and compatible with the low-temperature processing

requirement and is expected to be useful in other laser processing techniques on plastic, such as laser-assisted direct imprinting (LADI)^[25,26] via hole filling,^[27] catalyst metal-particle patterning,^[28,29] recrystallization of amorphous silicon films,^[30–32] and so on.

6. Experimental Section

The double-layer imprint resist consisted of underlayer resist NXR-3022 and top UV-curable resist NXR-2030, both from Nanonex Corp. NXR-3022 was spin coated and baked at 110 °C for 10 min, while NXR-2030 was not baked. The fused-silica pillar mold was pretreated with NXT-110 mold-release agent (Nanonex Corp.). NIL was carried out in a nanoimprinter (NX-2000, Nanonex Corp.).

Acknowledgements

We thank the Office of Naval Research (ONR), Defense Advanced Research Project Agent (DARPA), and National Science Foundation (NSF) for their partial support to the work, Ron Auberger in DuPont Teijin Films for providing the PET film samples, our colleague Dr. Zhihang Hu for discussion on COMSOL simulation, and Dr. Judy A. Swan in Princeton Writing Center for suggestions on draft revisions.

- [1] G. Gustafsson, Y. Cao, G. M. Treacy, F. Klavetter, N. Colaneri, A. J. Heeger, *Nature* **1992**, 357, 477–479.
- [2] C. D. Dimitrakopoulos, S. Purushothaman, J. Kymissis, A. Callegari, J. M. Shaw, *Science* **1999**, 283, 822–824.
- [3] J. A. Rogers, Z. Bao, K. Baldwin, A. Dodabalapur, B. Crone, V. R. Raju, V. Kuck, H. Katz, K. Amundson, J. Ewing, P. Drzaic, *Proc. Natl. Acad. Sci. USA* **2001**, 98, 4835–4840.
- [4] H. Gleskova, S. Wagner, V. Gasparik, P. Kovac, *J. Electrochem. Soc.* **2001**, 148, G370–G374.
- [5] C. J. Brabec, A. Cravino, D. Meissner, N. S. Sariciftci, T. Fromherz, M. T. Rispens, L. Sanchez, J. C. Hummelen, *Adv. Funct. Mater.* **2001**, 11, 374–380.
- [6] D. Hegemann, H. Brunner, C. Oehr, *Nucl. Instrum. Methods Phys. Res. Sect. B* **2003**, 208, 281–286.
- [7] M. Peter, F. Furthner, J. Deen, W. J. M. de Laat, E. R. Meinders, *Thin Solid Films* **2009**, 517, 3081–3086.
- [8] I. M. Ward, P. R. Pinnock, *Br. J. Appl. Phys.* **1966**, 17, 3–32.
- [9] D. R. Lide, *CRC Handbook of Chemistry and Physics*, <http://www.hbcpnetbase.com/>, **2009**.
- [10] H. Lee, S. H. Hong, K. Y. Yang, K. W. Choi, *Appl. Phys. Lett.* **2006**, 88, 143112.
- [11] C. M. Hessel, E. J. Henderson, J. G. C. Veinot, *Chem. Mater.* **2006**, 18, 6139–6146.
- [12] S. Y. Chou, P. R. Krauss, P. J. Renstrom, *Science* **1996**, 272, 85–87.
- [13] S. Y. Chou, P. R. Krauss, *Microelectron. Eng.* **1997**, 35, 237–240.
- [14] S. Y. Chou, Q. F. Xia, *Nat. Nanotechnol.* **2008**, 3, 295–300.
- [15] Q. Y. Tong, G. H. Cha, R. Gafiteanu, U. Gosele, *J. Microelectromech. Syst.* **1994**, 3, 29–35.

- [16] I. Junarsa, P. F. Nealey, *J. Vac. Sci. Technol. B* **2004**, *22*, 2685–2690.
- [17] P. T. Liu, T. C. Chang, S. M. Sze, F. M. Pan, Y. J. Mei, W. F. Wu, M. S. Tsai, B. T. Dai, C. Y. Chang, F. Y. Shih, H. D. Huang, *Thin Solid Films* **1998**, *332*, 345–350.
- [18] M. Kawamori, K. I. Nakamatsu, Y. Haruyama, S. Matsui, *Jpn. J. Appl. Phys. Part 1* **2006**, *45*, 8994–8996.
- [19] Q. F. Xia, S. Y. Chou, *Nanotechnology* **2008**, *19*, 455301.
- [20] B. J. Keene, *Int. Mater. Rev.* **1993**, *38*, 157–192.
- [21] M. K. Chaudhury, *Mater. Sci. Eng. R* **1996**, *16*, 97–159.
- [22] Plastics. Professional, Thermal Properties of Plastic Materials, <http://www.professionalplastics.com/professionalplastics/ThermalPropertiesofPlasticMaterials.pdf>, **2009**.
- [23] F. P. Incropera, D. P. DeWitt, *Fundamentals of Heat and Mass Transfer*, Wiley, New York **2002**, pp. 905–931.
- [24] K. Maex, M. R. Baklanov, D. Shamiryan, F. Iacopi, S. H. Brongersma, Z. S. Yanovitskaya, *J. Appl. Phys.* **2003**, *93*, 8793–8841.
- [25] S. Y. Chou, C. Keimel, J. Gu, *Nature* **2002**, *417*, 835–837.
- [26] Q. F. Xia, C. Keimel, H. X. Ge, Z. N. Yu, W. Wu, S. Y. Chou, *Appl. Phys. Lett.* **2003**, *83*, 4417–4419.
- [27] B. Cui, W. Wu, C. Keimel, S. Y. Chou, *Microelectron. Eng.* **2006**, *83*, 1547–1550.
- [28] J. Bosbach, D. Martin, F. Stietz, T. Wenzel, F. Trager, *Appl. Phys. Lett.* **1999**, *74*, 2605–2607.
- [29] Q. F. Xia, S. Y. Chou, *Nanotechnology* **2009**, *20*, 285310.
- [30] P. M. Smith, P. G. Carey, T. W. Sigmon, *Appl. Phys. Lett.* **1997**, *70*, 342–344.
- [31] J. S. Im, H. J. Kim, M. O. Thompson, *Appl. Phys. Lett.* **1993**, *63*, 1969–1971.
- [32] D. P. Gosain, T. Noguchi, S. Usui, *Jpn. J. Appl. Phys. Part 2* **2000**, *39*, L179–L181.

Received: January 23, 2010
Revised: March 15, 2010
Published online: May 6, 2010